doi:10.1017/S1431927622002057
Microsc. Microanal. 28 (Suppl 1), 2022

Multi-Axis Acquisition Schemes for Scalar and Vector Electron Tomography

George R. Lewis[1,2*], Emilie Ringe[1,2], Paul Midgley[1]

[1.] Department of Materials Science and Metallurgy, University of Cambridge, Cambridge, UK.
[2.] Department of Earth Sciences, University of Cambridge, Cambridge, UK.
* Corresponding author: grl31@cam.ac.uk

Electron tomography (ET) allows us to probe nanoscale morphologies and compositions in 3D with high spatial resolution [1]. In a typical scalar ET experiment, this is achieved by rotating the sample about a single axis and acquiring projection images at regular intervals, which can then be reconstructed to form a 3D representation. In magnetic vector ET it is common to rotate about a second perpendicular axis to allow for reconstruction of the magnetic field $\boldsymbol{B}$, since each projection is insensitive to the component of $\boldsymbol{B}$ parallel to the beam direction [2]. However, this regular sampling is not necessarily the optimum way to carry out an ET experiment, with reasons to explore alternative acquisition schemes including: anisotropic distributions of sample complexity; the need to reconstruct three perpendicular components in vector ET; and the fact that near-random sampling approaches may benefit reconstructions using compressed sensing regularisation. In this work we first build upon the well-known Crowther criterion to create a directional, vector-resolved resolution (DVR) prediction metric, and subsequently compare the performance of different acquisition schemes for both scalar and vector simulated ET experiments. Our results show that the DVR metric helps when designing tomography experiments, and that particularly for magnetic vector ET, multi-axis acquisition schemes may improve reconstruction quality.

The Crowther criterion is used to estimate the resolution d for a given number of projections N and object size D using $d \approx \pi D / N$, assuming full angular range about a single tilt axis [3]. This is a useful predictor for typical scalar ET experiments, but its applicability to more complex experiments is relatively limited due to its assumption of full angular range. We introduce here the DVR metric in an attempt to retain the intuitive interpretability of Crowther's resolution metric, whilst being compatible with vector experiments and accounting for the fact that different acquisition schemes generally have a directionally anisotropic performance. The first step in calculating the DVR metric is to represent the tilt scheme in reciprocal space using the Fourier slice theorem; the extent of each slice is determined by image sampling frequency (i.e. pixel width) and the thickness of each slice comes from the lowest frequency in the image (i.e. image width). In the next step we then consider the fractional data coverage ψ in Fourier space along a specific direction (defined by a cone with a chosen semi-angle of 15º) as a function of spatial frequency f (Figure 1a). At some point, the coverage ψ falls below 50%, signifying that the criteria for Nyquist sampling is no longer fulfilled in that direction (Figure 1b). By mapping this f_{50} resolution in all directions, we build up a directionally-resolved map of expected resolution (Figure 1c). In the case of vector ET, this process can be simply modified by creating a separate representation in Fourier space for each component of the magnetic field $\boldsymbol{B}$ and weighting the coverage of each slice by its sensitivity to the field component; we can then adjust our f_{50} criterion to include a threshold defining what sensitivity is sufficient for our desired magnetic fidelity (a value of ~0.71 is a good proxy, indicating the projection direction is within 45º of the most sensitive component) (Figure 1b).

Using the DVR metric we can predict situations in which multi-axis sampling may be beneficial. To explore this further we subsequently compared the reconstruction performance of several acquisition schemes (Figure 2a) in simulated scalar and vector ET experiments. In addition to the well-known

single, dual and quadruple tilt schemes, we also considered 'synchronised' (α and β tilts are varied proportionally to one another), conical (at several fixed values of α, the full range of β is scanned), and random tilt schemes. For scalar ET we tested a cavity-containing cuboid as a phantom (Figure 2b), with very limited tilt range and number of tilts, and found that in this scenario the synchronised acquisition scheme significantly outperforms single tilt schemes (Figure 2d). For vector ET we used a magnetic hopfion core (Figure 2c) as a phantom; and observed that for reconstructing the B_x and B_y components, there is little difference between dual-axis and other schemes. However, for the B_z component, dual-axis is significantly worse than all other tested multi-axis schemes, with the conical tilt scheme giving the best results (Figure 2e). This is due to a more uniform sampling of directions with the synchronised and conical tilt schemes, (the conical scheme works better for relatively large numbers of projections, which explains its worse performance in the scalar example, where only 16 images are used).

In conclusion, we have showcased a new metric for predicting ET resolution in multi-axis acquisition schemes and have shown through simulated experiments that there is a clear motivation for their use. This has potential to improve performance in scalar ET experiments where tilt range or dose are limiting factors, and in vector ET experiments where the B_z component is of particular interest [4].

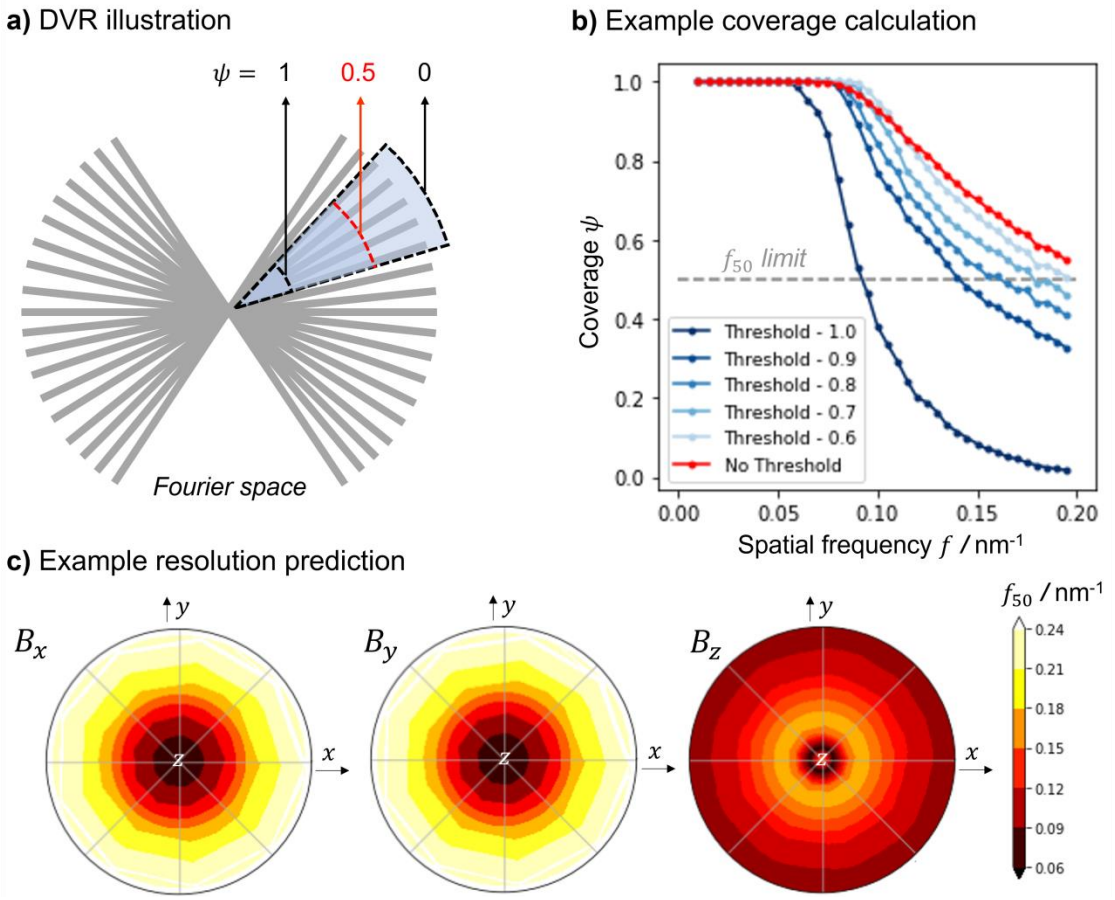

Figure 1. Directional vector-resolved resolution (DVR) prediction metric. (a) 2D illustration of the DVR calculation process. (b) Illustration of typical behaviour of $\psi(f)$, shown for B_x along [221] for an x-axis tilt scheme (20 projections between ±70º). (c) Resolution maps for a dual-axis tilt scheme (20 projections between ±70º for each axis). Polar plots show xy-plane resolutions at the circumference and z resolution in the centre. (b) and (c) assume input images of 100 nm width and 1 nm pixel spacing.

https://doi.org/10.1017/S1431927622002057 Published online by Cambridge University Press

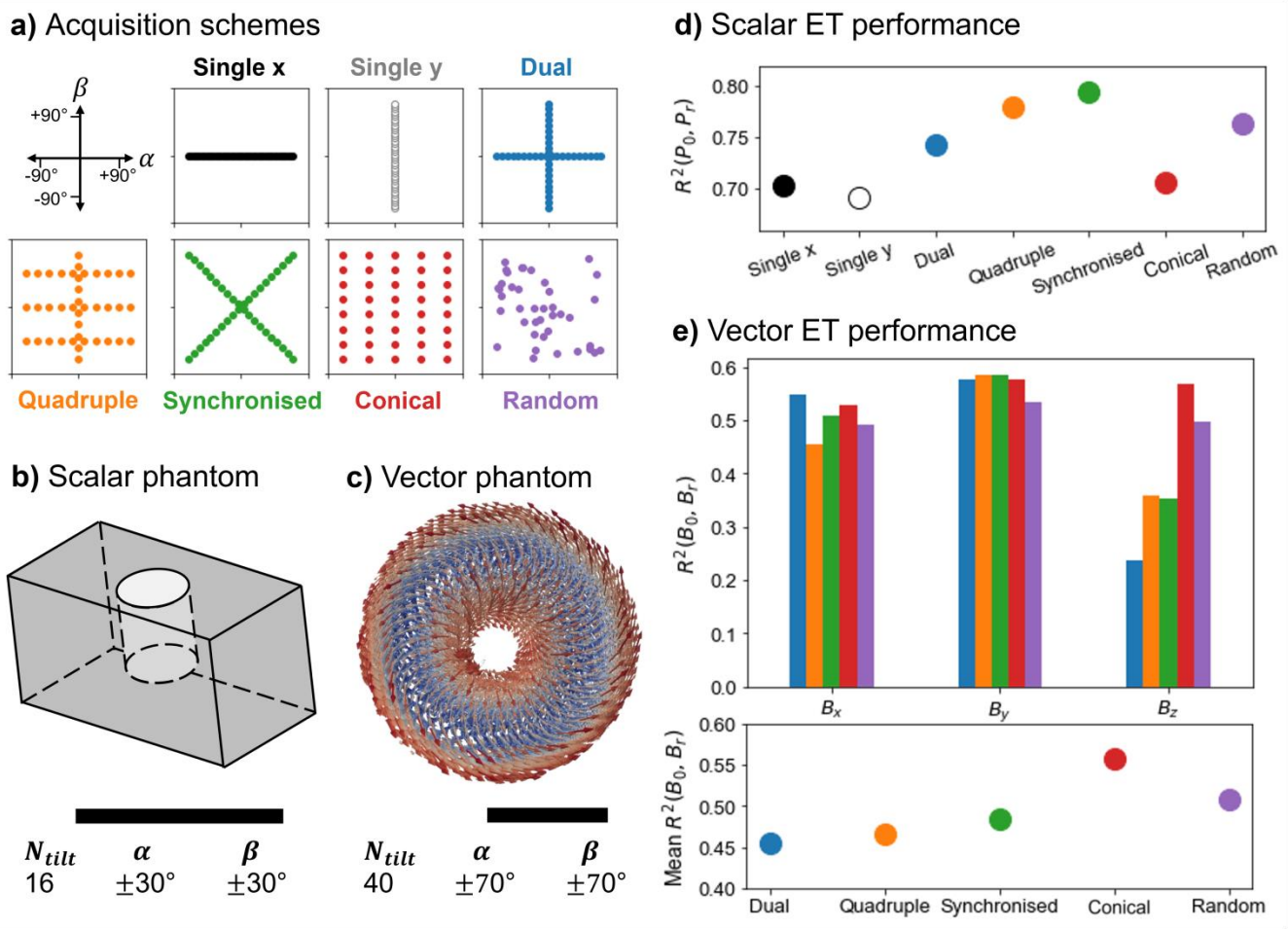

Figure 2. Multi-axis ET performance. (a) Illustration of seven acquisition schemes, represented by their distribution of tilt angles (shown for 40 projections with ±70º limits). (b) and (c) show our tested scalar phantom (a cuboid with a hollow cylindrical cavity) and vector phantom (magnetic hopfion core, here plotting $\boldsymbol{M}$); scalebars are 100 nm. (d) Scalar performance measured as the R^2 value between phantom P_0 and reconstruction P_r, reconstructed using a total variation regularisation algorithm. (e) Vector performance, shown as the R^2 value for each component of B (top) and mean average R^2 value (bottom), reconstructed using a wavelet regularisation algorithm. Colours in (d) and (e) correspond to labels in (a).

References:

[1] P.A. Midgley, and R.E. Dunun-Borkowski, *Nat. Mater.* **8** (2009) 271–279. doi:10.1038/NMAT2406.
[2] D. Wolf et al., *Nat. Nanotechnol. 2021*. (2021) 1–6. doi:10.1038/s41565-021-01031-x.
[3] R.A. Crowther, D.J. DeRosier, and A. Klug, *Proc. Roy. Soc. Lond. A.* **317** (1970) 319–340.
[4] We acknowledge support from the EPSRC NanoDTC Cambridge (EP/L015978/1) and EPSRC grants EP/V007750/1, EP/R008779/1 and EP/N032128/1.